Materials Science & Engineering A 764 (2019) 138222

Contents lists available at ScienceDirect

Materials Science & Engineering A

journal homepage: www.elsevier.com/locate/msea

The interplay between deformation mechanisms in austenitic 304 steel during uniaxial and equibiaxial loading

E. Polatidis[a,1], M. Šmíd[a], W.-N. Hsu[a,b], M. Kubenova[a], J. Capek[c], T. Panzner[c], H. Van Swygenhoven[a,b,*]

[a] Swiss Light Source, Paul Scherrer Institute, CH-5232, Villigen PSI, Switzerland
[b] Neutrons and X-rays for Mechanics of Materials, IMX, Ecole Polytechnique Federale de Lausanne, CH-1015, Lausanne, Switzerland
[c] Laboratory for Neutron Scattering and Imaging, Paul Scherrer Institute, CH-5232, Villigen PSI, Switzerland

ARTICLE INFO

Keywords:
Neutron diffraction
Twinning
Martensite
Steel
Multiaxial

ABSTRACT

The preferred deformation mechanisms with respect to the load path are studied in a medium stacking fault energy 304 austenitic stainless steel that exhibits both transformation induced plasticity and twinning induced plasticity. In situ neutron diffraction and post-mortem EBSD show that the transformation from γ-austenite to α′-martensite is facilitated by equibiaxial loading rather than uniaxial loading. The results are discussed with respect to the evolving crystallographic texture, the presence of deformation twins and martensite under the different load paths. The evolving crystallographic texture under uniaxial loading favors the deformation twinning and delays the martensitic transformation. In contrast, under equibiaxial loading the strain is accommodated by slip along multiple slip planes, which provide nucleation sites for martensitic transformation. It is found that the preferred deformation mechanism is not only an inherent property related to the stacking fault energy, but it also greatly depends on the load path and the deformation texture.

1. Introduction

Contradicting reports have been published on the influence of the loading state on the martensitic transformation. Some studies report that uniaxial loading facilitates the deformation-induced martensitic transformation [1,2], others show that the martensitic transformation is favored under biaxial loading [3,4]. The loading state has been taken into account in martensite kinetic models by scalar variables [1,5]. A more recent physically-driven model implemented in an elasto-plastic (EPSC) framework accounts for the effect of load path by modeling the splitting of the Shockley partial dislocations (SPDs) as a precursor for the martensitic transformation [6]. However, the above mentioned kinetic models neglect the interaction of several co-existing deformation mechanisms, such as transformation induced plasticity (TRIP) and/or twinning induced plasticity (TWIP), and assume a single deformation mechanism regardless the load path (i.e. only martensitic transformation).

The stacking fault energy (SFE) of an austenitic stainless steel strongly influences the preferred deformation mechanisms [7]. It has been generally observed that with increasing the SFE, the deformation mechanisms gradually change from martensitic phase transformations (TRIP) [2,8,9] to mechanical twinning (TWIP) [9,10] and plasticity only by dislocation slip [9].

The effect of uniaxial/biaxial loading on the martensitic transformation of a low SFE austenitic steel was studied by in-situ neutron diffraction [2]. It was shown that uniaxial loading favors the martensitic transformation following the sequence $\gamma \rightarrow \varepsilon \rightarrow \alpha'$, where at low strains ε-martensite is the precursor of α′-martensite. During equibiaxial-loading however, the evolving texture suppresses the formation of ε-martensite and considerably less α′-martensite is observed at high strains. It was shown that the grains containing martensite belong to orientations for which the leading partial dislocation (LPD) has a higher Schmid factor than the trailing partial dislocation (TPD). The martensitic transformation is suppressed during equibiaxial loading as a consequence of the different texture formed during deformation, as compared to uniaxial loading.

In materials with higher SFE, for which nucleation and growth of twins is observed [11,12], several models have been proposed for the nucleation of twins as a result of dislocation interactions [13–15]. As the growth of twins is described by the glide of Shockley partial dislocations (SPDs), the precursor for twin growth is the separation of the SPDs under an external load [16,17] and the difference in the stress

* Corresponding author. Swiss Light Source, Paul Scherrer Institute, CH-5232, Villigen PSI, Switzerland.
E-mail address: helena.vanswygenhoven@psi.ch (H. Van Swygenhoven).
[1] Currently: Laboratory for Neutron Scattering and Imaging, Paul Scherrer Institute, CH-5232, Villigen PSI, Switzerland.

https://doi.org/10.1016/j.msea.2019.138222
Received 22 May 2019; Received in revised form 24 July 2019; Accepted 25 July 2019
Available online 26 July 2019

between the LPD and the TPD has been also applied to explain the growth of twins [18].

Some steels with appropriate compositions/SFEs exhibit a combination of TWIP/TRIP effects [9,18–20]. It has been observed experimentally that twins form at lower strains than α′-martensite [18,21,22], and the intercepts of twins with other planar defects can act as nucleation sites for α′-martensite with increasing the applied strain [21]. A study on medium-Mn maraging steels [23] reported the competition between twinning and martensite formation: large grains exhibited only twinning whereas smaller grains only the martensitic transformation.

The aim of this study is to compare the interplay of the deformation mechanisms in a nearly randomly textured, before deformation, austenitic 304 steel with medium SFE under monotonic uniaxial and equibiaxial loading. The deformation mechanisms (TWIP and/or TRIP) are discussed with respect to the load path and the evolving crystallographic texture.

2. Materials and methods

A commercial AISI304 (EN 1.4301) stainless steel with composition shown in Table 1 in sheet form of 8 mm thickness was purchased from SAUTER EDELSTAHL AG, Switzerland.

The inverse pole figure (IPF) map along the normal direction (ND) in Fig. 1 shows the initial microstructure exhibiting equiaxed grains with relatively random crystallographic texture (also shown in the IPFs in Fig. 4-a). The average grain size (excluding the annealing twins) is 35 μm. In situ neutron diffraction studies were carried out at the POLDI instrument of the Swiss neutron spallation source, SINQ, (Paul Scherrer Institute, Switzerland) using the biaxial deformation rig [2,24]. Cruciform-shaped samples with the geometry proposed in Ref. [24] were used for the equibiaxial tests.

For the uniaxial loading, dogbone-shaped samples with the geometry given in Ref. [25] were used. The biaxial deformation system is equipped with a 2-camera digital image correlation (DIC) system (GOM, Aramis 5 M) for measuring the in-plane strain at the center of the cruciform sample. Uniaxial loading and equibiaxial loading were performed with a loading rate of 80 N/s. The uniaxial loading direction was parallel to the rolling direction of the sheet (RD), and the equibiaxial load was applied along the RD and the second in-plane, hereafter called, transverse direction (TD). The neutron diffraction measurements were carried out in predefined force intervals after interrupting the loading and holding the displacement. The maximum equivalent strain reached during the equibiaxial and uniaxial tests were ~28% and ~26% respectively. For studying the uniaxial deformation under high strain, an additional dogbone sample was deformed up to 41.9% (true) strain with the uniaxial test rig of the POLDI instrument. The neutron diffraction data were reduced and fitted using the open source software Mantid [26].

EBSD studies were carried out on the as-received and on the deformed material by extracting samples from the center of the deformed cruciform and dogbone samples. The samples were ground with 1200 grit SiC paper and then electropolished for 12 s with a 16:3:1 (by volume) ethanol, glycerol and perchloric acid solution at 42 V. A field emission gun scanning electron microscope (FEG SEM) Zeiss ULTRA 55 equipped with EDAX Hikari Camera operated at 20 kV in high current mode with 120 μm aperture was used. The EBSD raw data was post-processed using the EDAX OIM Analysis 7.3 software.

High-resolution digital image correlation (HR-DIC) was performed in an SEM on miniaturized cruciform samples under uniaxial and equibiaxial load paths. A detailed description of the sample preparation, experimental and analysis of the HR-DIC data is given in Ref. [27].

Table 1
Chemical composition of the studied steel as provided by the supplier (maximum in wt.%, unless a range is given).

C	Si	Mn	P	S	Ni	Cr	N	Fe
0.07	1.00	2.00	0.045	0.015	8–10.5	17.5–19.5	0.11	Bal.

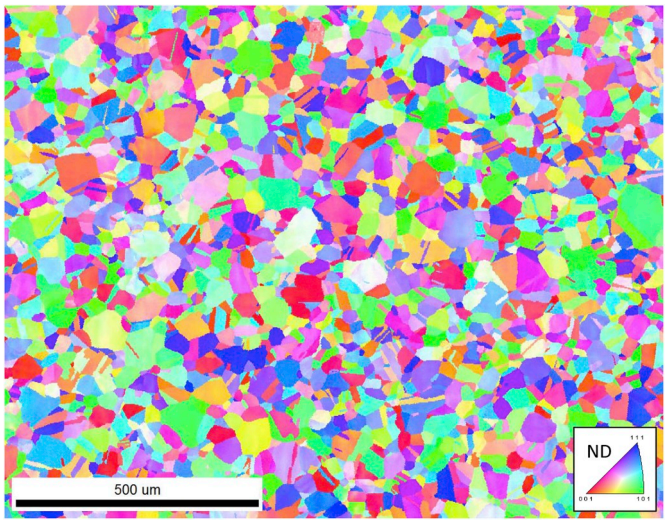

Fig. 1. IPF map along the ND direction of the as-received sheet.

3. Results

3.1. Phase transformation

The mechanical data from both uniaxial and equibiaxial load paths are given in Fig. 2-a and -c, the resulting force is calculated as in Ref. [27]. Evaluating the stress state at the center of a cruciform-shaped specimen is not as straightforward as for a dogbone-shaped specimen (given in Fig. 2-a) since the cruciform sample does not have a well-defined cross-section [24,27,28]. Instead, finite element (FE) simulations can give a good estimate of the stress state in the middle of the cruciform, as presented in Ref. [27]. For this simulation, the stress-strain curve and isotropic elastic properties of the material, obtained from the uniaxial test, are used as materials properties input to the built-in model based on the Von Mises yield criterion and the associated flow rule in ABAQUS. Fig. 2-c shows the FE prediction for the equivalent stress at the center of the cruciform.

The neutron data are collected while keeping the displacement fixed and letting the sample to relax, as shown by the red points on the force-strain curve. Martensite reflections do not appear in the neutron diffraction patterns during uniaxial deformation up to 26% strain, as shown in Fig. 2-a and -b. By continuing straining the uniaxial loaded sample to 41.9% strain, α′-martensite appears at strains above approximately 30%. Fig. 3 shows the increasing intensity of the 110_{BCC} reflection of α′-martensite as the strain increases. In contrast to uniaxial loading, new reflections corresponding to the α′-martensite phase, i.e. 110_{BCC} and 211_{BCC}, appear already at approximately 15% of equivalent strain under equibiaxial loading, as shown in Fig. 2-c and -d. The equibiaxial loading facilitates the formation of α′-martensite and the transformation is seen to occur from austenite directly to α′-martensite, i.e. γ→α′. The austenite/martensite diffraction intensity fraction and the mechanical behavior of these samples were used as input in the model development in Ref. [6].

3.2. Crystallographic texture

Different crystallographic textures develop during uniaxial and equibiaxial deformation [2]. The nearly random crystallographic texture of the as-received material (Fig. 4-a) evolves to a strong < 111 > -

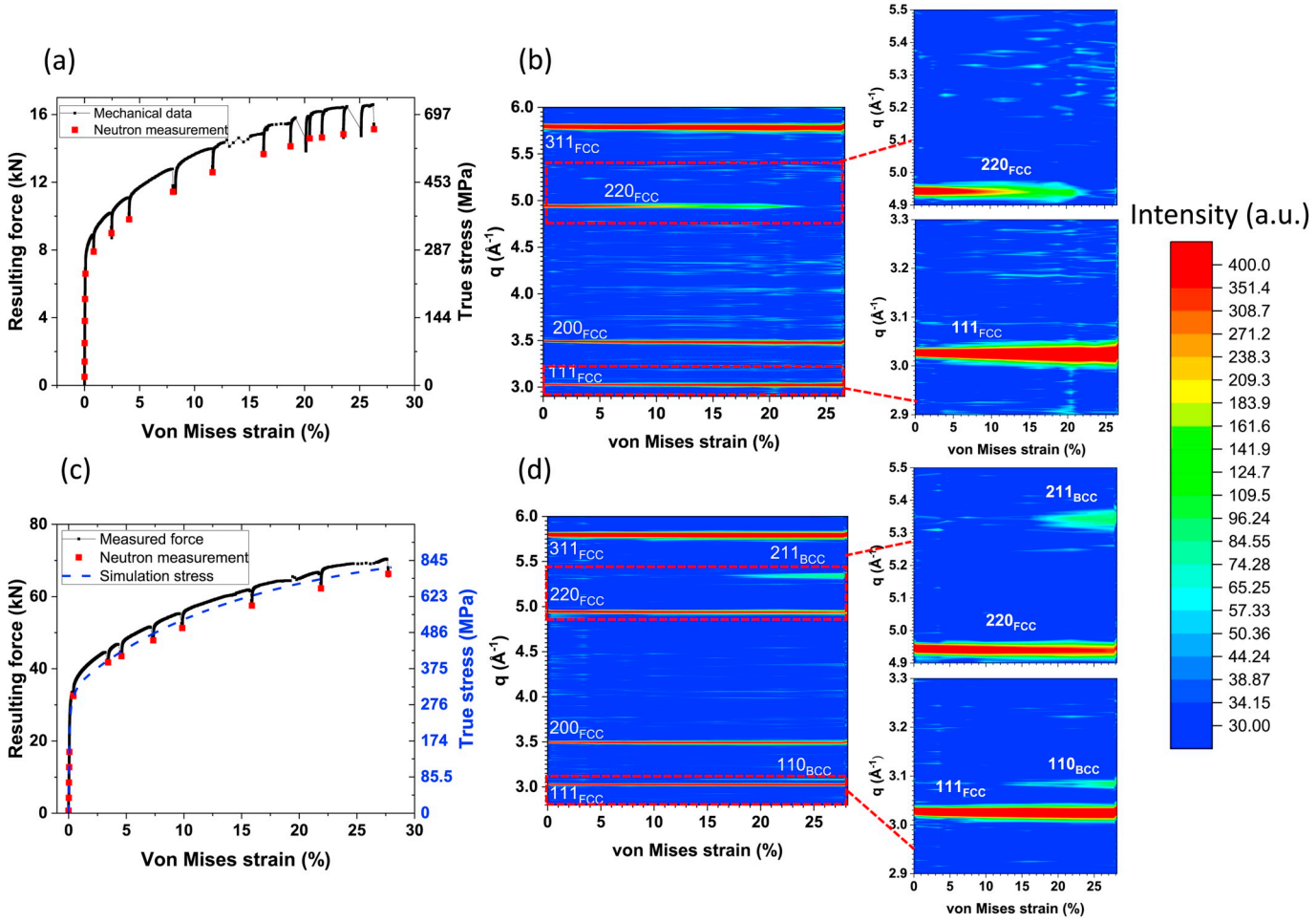

Fig. 2. Force/stress-strain plots and the evolution of the neutron diffraction patterns with increasing strain for a) uniaxial loading c) equibiaxial loading. The red points indicate the strain values at which neutron measurements where conducted. The corresponding neutron diffraction patterns (b) and (d) as a function of von Mises strain. Parts of the q range are magnified showing the appearance of martensite under equibiaxial loading at strain higher than 15%. No martensite formation can be observed under uniaxial loading. (For interpretation of the references to color in this figure legend, the reader is referred to the Web version of this article.)

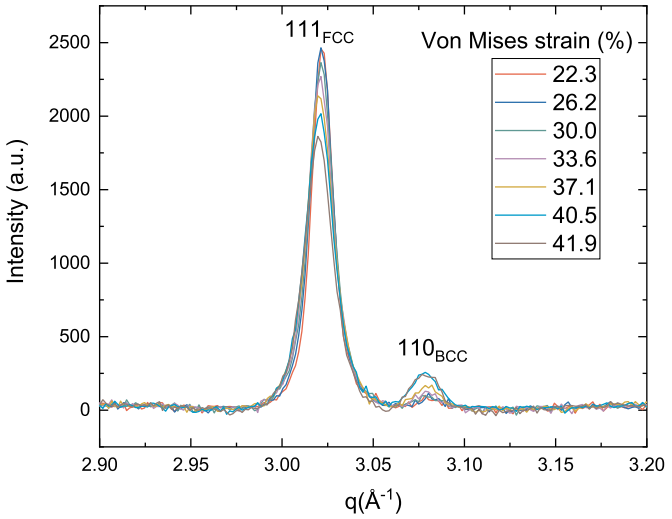

Fig. 3. Sequence of neutron diffraction patterns under uniaxial loading (at strains from 22.3% to 41.9% true strain) showing the increasing intensity of the 110_{BCC} α′-martensite reflection at higher strain.

texture along the loading direction (LD) that is parallel to the RD during uniaxial loading. Meanwhile the < 110 > -texture weakens along the loading direction (LD), as shown in Fig. 4-b, and as also seen in Fig. 2-b where the 220_{FCC} refelction almost disappears at strains higher than approximately 20%. The in-plane equibiaxial loading has the same normalized strain tensor as uniaxial compression along ND [24] and it results in a typical < 110 > -texture along the out-of-plane direction (Fig. 4-c) [2,29–31].

Fig. 5 shows the grain orientation maps after uniaxial (the IPF is given along RD) and equibiaxial (the IPF is given along ND) loading. The austenite grains with crystallographic orientations for which the LPDs experience higher stress than the TPDs i.e. the splitting distance between the SPDs increases, are colored blue, while the rest of the orientations are colored red and α′-martensite is shown in yellow. It is observed that after uniaxial deformation (Fig. 5-a) most grains favor the splitting of the SPDs (most grains are blue), however a very small fraction of martensite forms in both red and blue grains. The low volume fraction of martensite under uniaxial loading explains why martensite is not detected by neutron diffraction before 30% strain is reached (shown in Fig. 3). Under equibiaxial loading, the majority of α′-martensite forms in the grains which do not favor the splitting of the SPDs (red grains) as shown in Fig. 5-b. The difference in martensitic transformation between uniaxial and biaxial deformation in this

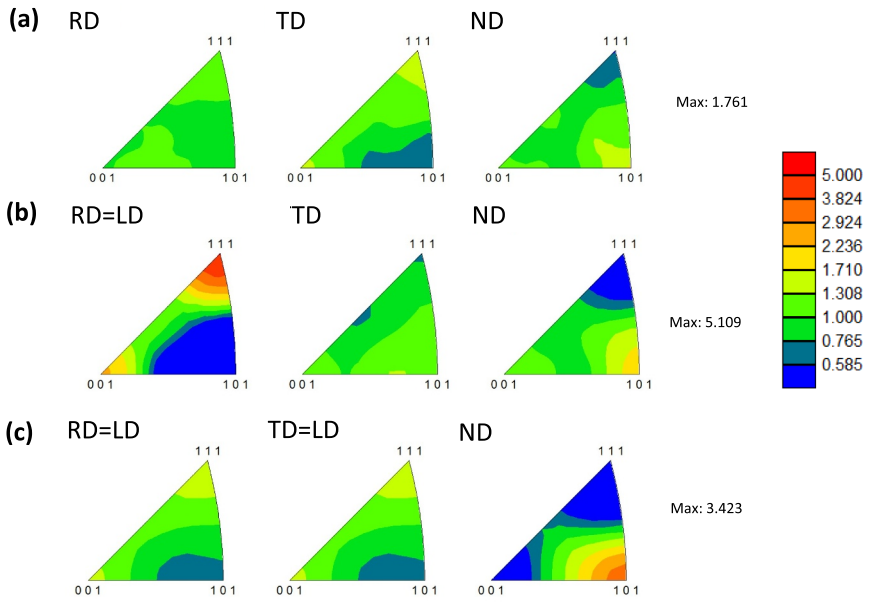

Fig. 4. IPFs along the 3 principal sample directions showing (a) the nearly random crystallographic texture of the initial state of the material and the deformation textures after (b) uniaxial (c) equibiaxial loading.

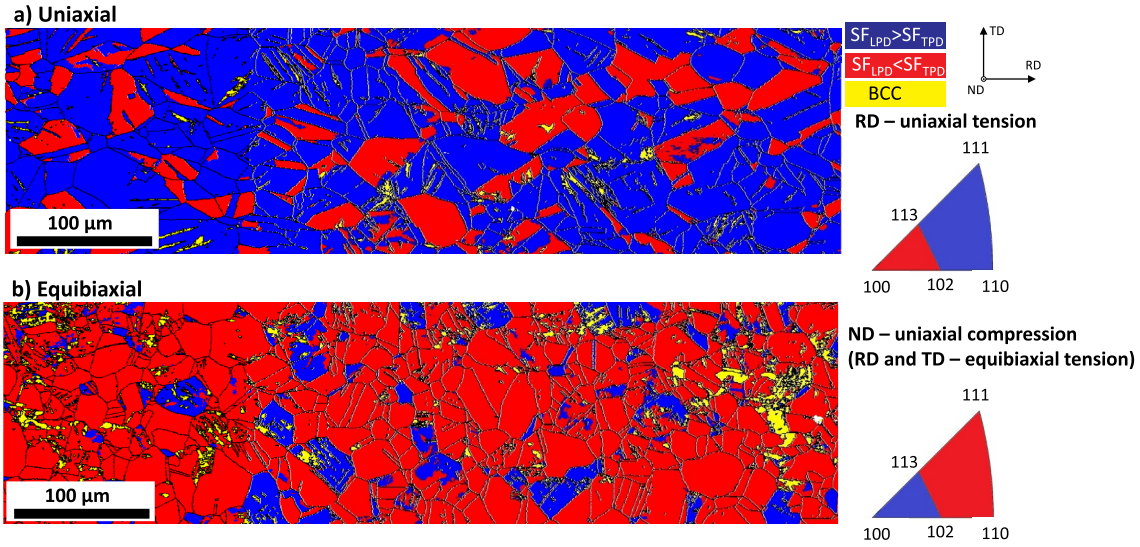

Fig. 5. Post mortem EBSD maps, color-coded for showing austenite orientations that favor the splitting of the SPDs (blue) or not (red) and strain-induced α′-martensite (yellow) for the sample deformed a) uniaxially in the direction parallel to the RD, and b) equibiaxially (equivalent to compression in the ND direction). The IPF triangles show which orientations favor splitting of the SPDs under uniaxial and equibiaxial loading. (For interpretation of the references to color in this figure legend, the reader is referred to the Web version of this article.)

medium SFE material cannot be explained by the difference in stress experienced by the LPD and TPD, as was the case for the low SFE material where ε-martensite formed upon deformation [2].

3.3. Twinning

Twinning, as another possible deformation mechanism in medium SFE steels, is also influenced by the stresses experienced by the SPDs. In the EBSD map shown in Fig. 6-a, grains favorably oriented for splitting of the SPDs under uniaxial loading are marked as A, B, C, D. The orientation of these grains is given in Fig. 6-b. Deformation twins are seen in these grains. For instance in grain D, a characteristic misorientation of 60° relative to the parent grain is measured (plotted in Fig. 2-c) along the dashed line shown in -Fig. 2-a. Fig. 7 shows a similar analysis for a grain favorably oriented for twinning in the sample deformed under equibiaxial loading. The EBSD map (Fig. 7-a) collected at high magnification shows several twins in grain (E); martensite is given in yellow. As these EBSD maps (Figs. 6 and 7) are collected after deformation, a significant gradient in orientation is seen within each grain. The orientation distribution of the chosen grains given in Figs. 6-b and 7-b, is however within the range of favorable orientations for twinning for both load paths.

The majority of the grains in the sample deformed under uniaxial loading favor the formation of deformation twins. Some grains with either favorable and non-favorable orientation for twinning contain martensite showing that the deformation twinning does not suppress the formation of martensite but it rather retards it. Fig. 6-a illustrates that α′-martensite can form at twin boundaries and/or intercepts with

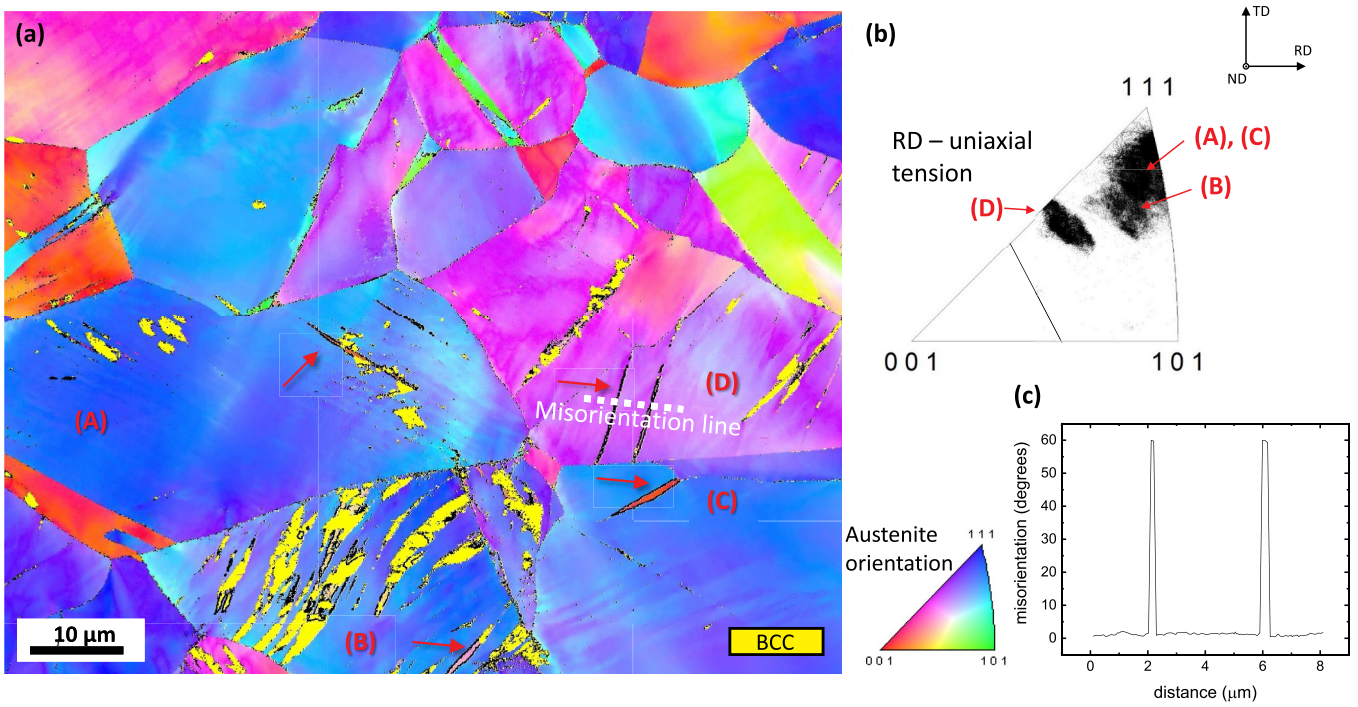

Fig. 6. Detailed IPF map of austenite in the direction parallel to the loading direction (RD), showing grains (labelled A, B, C, D) with deformation twins (shown with red arrows). The orientation distribution of these grains is shown in (b). (c) Misorientation plot along the line drawn in (a). The yellow subgrains in grains (A), (B) and (D) are martensite. The yellow color does not represent the grain orientation of α′-martensite (BCC). (For interpretation of the references to color in this figure legend, the reader is referred to the Web version of this article.)

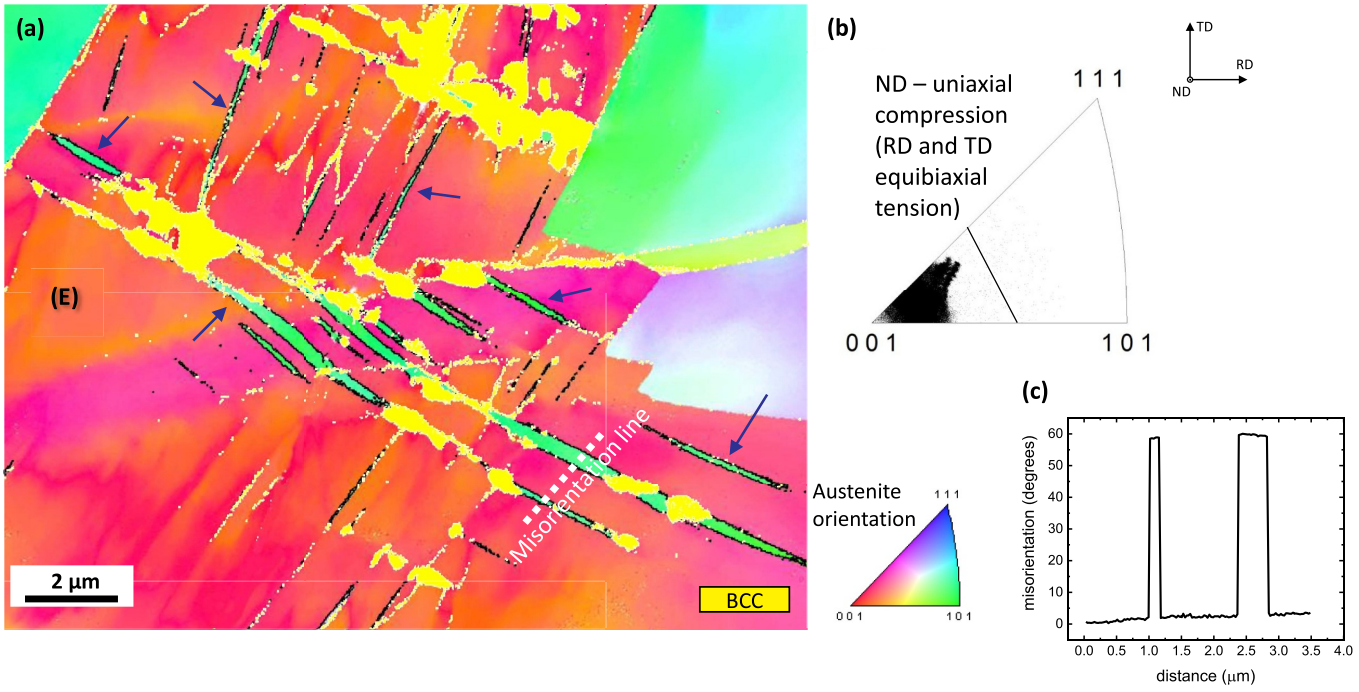

Fig. 7. Detailed IPF map in the direction perpendicular to the sample surface (ND), showing a grain with deformation twins (twins indicated with blue arrows) under equibiaxial loading. The orientation distribution of grain (E) is shown in (b). (c) Misorientation plot along the line drawn in (a). The yellow subgrains in grain (A) are martensite. The yellow color does not represent the grain orientation of α′-martensite (BCC). (For interpretation of the references to color in this figure legend, the reader is referred to the Web version of this article.)

other planar defects, such martensite is seen in grains (A) and (B).

In a previous study we demonstrated that high resolution digital image correlation can distinguish the slip activity under uniaxial and equibiaxial loading [27]. A more detailed examination of the crystallographic orientations of the grains within the field of view presented in Ref. [27], shows that the activation of slip in multiple slip planes is observed more frequently in the grains that do not favor twinning than those favorably oriented for twinning. In contrast, the grains with crystallographic orientations favorable for twinning, exhibit mostly slip on a single slip plane. Fig. 8-a shows a grain, favorably orientated for

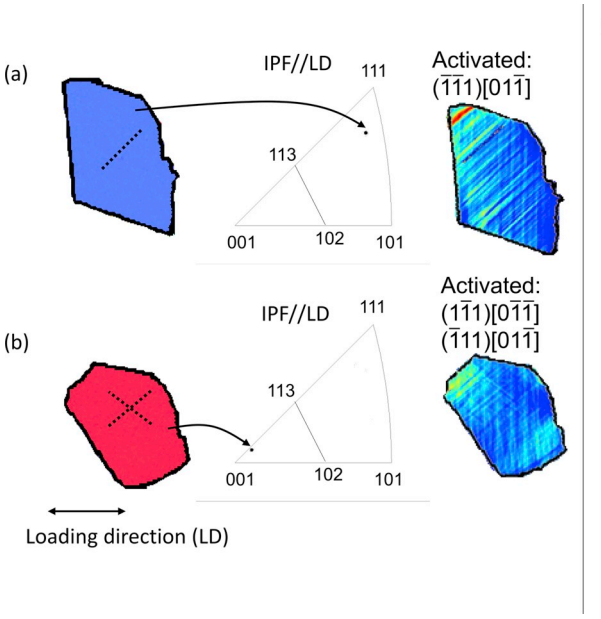

Fig. 8. HR-DIC maps showing (a) an example of a grain with favorable orientation (before loading) for twinning (via splitting of the PDs) under uniaxial loading exhibiting slip on a single slip plane; (b) an example of a grain with a non-favorable orientation for twinning under uniaxial loading exhibiting slip on two slip planes. The IPFs in (a) and (b) are given along the loading direction. (c) Statistical analysis (including the grains deformed under both uniaxial and equibiaxial loading) showing that more grains non-favorably orientated for splitting of the SPDs (red grains in Fig. 5) exhibit slip on multiple slip planes, whereas the favorably-oriented grains for splitting of the SPDs exhibit predominantly slip along only one slip plane (blue grains in Fig. 5). (For interpretation of the references to color in this figure legend, the reader is referred to the Web version of this article.)

splitting of the SPDs (favorable for twinning), where only one slip system is activated under uniaxial loading; Fig. 8-b shows a grain, non-favorably orientated for splitting of the SPDs, where two slip systems are activated under uniaxial loading. The statistical analysis of the slip behavior under both uniaxial and equibiaxial loading is plotted in Fig. 8-c for grains favorably and non-favorably for twinning. This result suggests that twinning suppresses the activation of slip on secondary slip planes, thus it suppresses the formation of shear band intercepts which are potential nucleation sites for martensite. The above-explained theory is valid for approximately 60–65% of the grains, whereas the observed discrepancy for the rest of the grains can be explained as follows. At the strain level (14% macroscopic strain) reached in Ref. [27], grain interactions and grain rotations can cause local stress variations so that the local stress state may not coincide with the macroscopically applied load [32]. This can locally affect the activation/suppression of secondary planes for slip.

4. Discussion and conclusion

The metastable austenitic 304 stainless steel was studied under uniaxial and equibiaxial load paths in situ with neutron diffraction. Equibiaxial loading facilitates the martensitic transformation following a direct path of γ-austenite to α′-martensite, whereas under uniaxial deformation the phase transformation is delayed. The sequence of the deformation mechanisms is schematically summarized in Fig. 9.

Under both strain paths, the deformation starts with single slip but after enough straining a < 111 > -texture and a < 110 > -texture is formed under uniaxial and equibiaxial deformation respectively. Under an evolving < 111 > -texture, the majority of the grains become favorably oriented for splitting of the partial dislocations and extended stacking faults and mechanical twinning form (steps 2–3 in Fig. 9), restricting the activation of slip on secondary slip planes. The lack of intersections of slip systems, which can serve as potential nucleation sites for α′-martensite, retards the phase transformation. Under biaxial loading, the evolving < 110 > -texture does not result in grain orientations that favor twinning, therefore slip on multiple slip planes starts allowing an early formation of α′-martensite at the slip intersections (steps 2–3 in Fig. 9). These results suggest that the TRIP/TWIP effects are not only dependent on the SFE, but they can be favored/suppressed under specific combinations of load path/crystallographic texture.

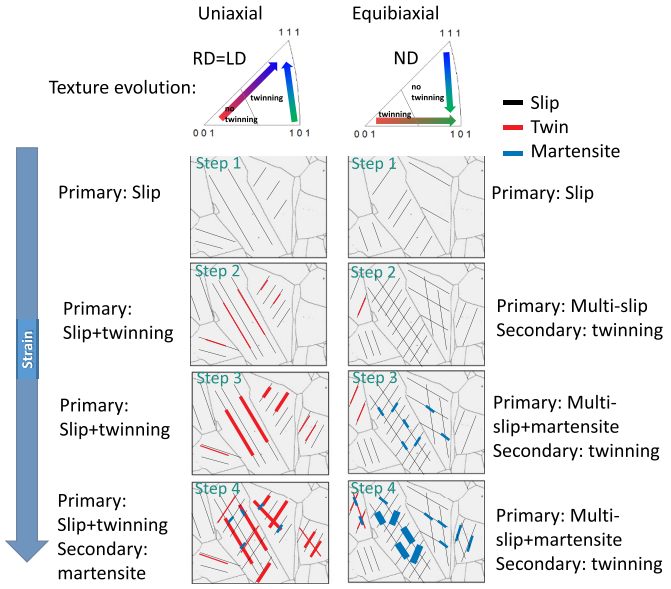

Fig. 9. The proposed sequence of the dominant deformation mechanisms under uniaxial and equibiaxial loading with increasing the applied strain. The IPFs at the top illustrate the evolution of deformation texture for the two load paths, i.e. strong < 111 > -texture along the loading direction for uniaxial loading and strong < 110 > -texture along the normal to the sample surface for equibiaxial loading.

Data availability

The raw/processed data required to reproduce these findings cannot be shared at this time as the data also forms part of an ongoing study.

Acknowledgment

EP, W–NH, MS, MK and HVS acknowledge the financial support from the European Research Council under the ERC advanced Grant MULTIAX (339245).

References

[1] A.M. Beese, D. Mohr, Effect of stress triaxiality and Lode angle on the kinetics of strain-induced austenite-to-martensite transformation, Acta Mater. 59 (2011) 2589–2600, https://doi.org/10.1016/j.actamat.2010.12.040.

[2] E. Polatidis, W.-N. Hsu, M. Šmíd, T. Panzner, S. Chakrabarty, P. Pant, H. Van Swygenhoven, Suppressed martensitic transformation under biaxial loading in low stacking fault energy metastable austenitic steels, Scr. Mater. 147 (2018) 27–32, https://doi.org/10.1016/j.scriptamat.2017.12.026.

[3] S.S. Hecker, M.G. Stout, K.P. Staudhammer, J.L. Smith, Effects of strain state and strain rate on deformation-induced transformation in 304 stainless steel: Part I, Magn. Meas. Mech. Behav., MTA. 13 (1982) 619–626, https://doi.org/10.1007/BF02644427.

[4] H.Y. Yu, G.Y. Kai, M. De Jian, Transformation behavior of retained austenite under different deformation modes for low alloyed TRIP-assisted steels, Mater. Sci. Eng. 441 (2006) 331–335, https://doi.org/10.1016/j.msea.2006.08.061.

[5] R.G. Stringfellow, D.M. Parks, G.B. Olson, A constitutive model for transformation plasticity accompanying strain-induced martensitic transformations in metastable austenitic steels, Acta Metall. Mater. 40 (1992) 1703–1716, https://doi.org/10.1016/0956-7151(92)90114-T.

[6] M. Zecevic, M.V. Upadhyay, E. Polatidis, T. Panzner, H. Van Swygenhoven, M. Knezevic, A crystallographic extension to the Olson-Cohen model for predicting strain path dependence of martensitic transformation, Acta Mater. 166 (2019) 386–401, https://doi.org/10.1016/j.actamat.2018.12.060.

[7] S. Allain, J.-P. Chateau, O. Bouaziz, S. Migot, N. Guelton, Correlations between the calculated stacking fault energy and the plasticity mechanisms in Fe–Mn–C alloys, Mater. Sci. Eng. 387–389 (2004) 158–162, https://doi.org/10.1016/j.msea.2004.01.059.

[8] P. Behjati, A. Najafizadeh, Role of chemical driving force in martensitic transformations of high-purity Fe-Cr-Ni alloys, Metall. Mater. Trans. A 42 (2011) 3752, https://doi.org/10.1007/s11661-011-0769-x.

[9] S. Martin, S. Wolf, U. Martin, L. Krüger, D. Rafaja, Deformation mechanisms in austenitic TRIP/TWIP steel as a function of temperature, Metall. Mater. Trans. A 47 (2016) 49–58, https://doi.org/10.1007/s11661-014-2684-4.

[10] K. Sato, M. Ichinose, Y. Hirotsu, Y. Inoue, Effects of deformation induced phase transformation and twinning on the mechanical properties of austenitic Fe–Mn–Al alloys, ISIJ Int. 29 (1989) 868–877, https://doi.org/10.2355/isijinternational.29.868.

[11] G.B. Olson, M. Cohen, A general mechanism of martensitic nucleation: Part I. General concepts and the FCC → HCP transformation, MTA 7 (1976) 1897–1904, https://doi.org/10.1007/BF02659822.

[12] J.W. Christian, S. Mahajan, Deformation twinning, Prog. Mater. Sci. 39 (1995) 1–157, https://doi.org/10.1016/0079-6425(94)00007-7.

[13] J.A. Venables, Deformation twinning in face-centred cubic metals, Philos. Mag.: A J. Theoret. Exp. Appl. Phys. 6 (1961) 379–396, https://doi.org/10.1080/14786436108235892.

[14] S. Mahajan, G.Y. Chin, Formation of deformation twins in f.c.c. crystals, Acta Metall. 21 (1973) 1353–1363, https://doi.org/10.1016/0001-6160(73)90085-0.

[15] H. Fujita, T. Mori, A formation mechanism of mechanical twins in F.C.C. Metals, Scr. Metall. 9 (1975) 631–636, https://doi.org/10.1016/0036-9748(75)90476-7.

[16] I. Karaman, H. Sehitoglu, K. Gall, Y.I. Chumlyakov, H.J. Maier, Deformation of single crystal Hadfield steel by twinning and slip, Acta Mater. 48 (2000) 1345–1359, https://doi.org/10.1016/S1359-6454(99)00383-3.

[17] T.S. Byun, On the stress dependence of partial dislocation separation and deformation microstructure in austenitic stainless steels, Acta Mater. 51 (2003) 3063–3071, https://doi.org/10.1016/S1359-6454(03)00117-4.

[18] C. Ullrich, R. Eckner, L. Krüger, S. Martin, V. Klemm, D. Rafaja, Interplay of microstructure defects in austenitic steel with medium stacking fault energy, Mater. Sci. Eng. 649 (2016) 390–399, https://doi.org/10.1016/j.msea.2015.10.021.

[19] H. Ding, Z.-Y. Tang, W. Li, M. Wang, D. Song, Microstructures and mechanical properties of Fe-Mn-(Al, Si) TRIP/TWIP steels, J. Iron Steel Res., Int. 13 (2006) 66–70, https://doi.org/10.1016/S1006-706X(06)60113-1.

[20] D. Borisova, V. Klemm, S. Martin, S. Wolf, D. Rafaja, Microstructure defects contributing to the energy absorption in CrMnNi TRIP steels, Adv. Eng. Mater. 15 (2013) 571–582, https://doi.org/10.1002/adem.201200327.

[21] Y.F. Shen, X.X. Li, X. Sun, Y.D. Wang, L. Zuo, Twinning and martensite in a 304 austenitic stainless steel, Mater. Sci. Eng. 552 (2012) 514–522, https://doi.org/10.1016/j.msea.2012.05.080.

[22] H.E. Sabzi, A. Zarei-Hanzaki, H.R. Abedi, A. Mateo, J.J. Roa, The sequential twinning-transformation induced plasticity effects in a thermomechanically processed high Mn austenitic steel, Mater. Sci. Eng. 725 (2018) 242–249, https://doi.org/10.1016/j.msea.2018.03.102.

[23] M.-M. Wang, C.C. Tasan, D. Ponge, A. Kostka, D. Raabe, Smaller is less stable: size effects on twinning vs. transformation of reverted austenite in TRIP-maraging steels, Acta Mater. 79 (2014) 268–281, https://doi.org/10.1016/j.actamat.2014.07.020.

[24] S. Van Petegem, J. Wagner, T. Panzner, M.V. Upadhyay, T.T.T. Trang, H. Van Swygenhoven, In-situ neutron diffraction during biaxial deformation, Acta Mater. 105 (2016) 404–416, https://doi.org/10.1016/j.actamat.2015.12.015.

[25] M.V. Upadhyay, T. Panzner, S. Van Petegem, H. Van Swygenhoven, Stresses and strains in cruciform samples deformed in tension, Exp. Mech. 57 (2017) 905–920, https://doi.org/10.1007/s11340-017-0270-6.

[26] O. Arnold, J.C. Bilheux, J.M. Borreguero, A. Buts, S.I. Campbell, L. Chapon, M. Doucet, N. Draper, R. Ferraz Leal, M.A. Gigg, V.E. Lynch, A. Markvardsen, D.J. Mikkelson, R.L. Mikkelson, R. Miller, K. Palmen, P. Parker, G. Passos, T.G. Perring, P.F. Peterson, S. Ren, M.A. Reuter, A.T. Savici, J.W. Taylor, R.J. Taylor, R. Tolchenov, W. Zhou, J. Zikovsky, Mantid—data analysis and visualization package for neutron scattering and μ SR experiments, Nucl. Instrum. Methods Phys. Res. Sect. A Accel. Spectrom. Detect. Assoc. Equip. 764 (2014) 156–166, https://doi.org/10.1016/j.nima.2014.07.029.

[27] E. Polatidis, W.-N. Hsu, M. Šmíd, H. Van Swygenhoven, A high resolution digital image correlation study under multiaxial loading, Exp. Mech. 59 (3) (2018) 309–317, https://doi.org/10.1007/s11340-018-00443-6.

[28] M.V. Upadhyay, S. Van Petegem, T. Panzner, R.A. Lebensohn, H. Van Swygenhoven, Study of lattice strain evolution during biaxial deformation of stainless steel using a finite element and fast Fourier transform based multi-scale approach, Acta Mater. 118 (2016) 28–43, https://doi.org/10.1016/j.actamat.2016.07.028.

[29] O. Engler, V. Randle, Introduction to Texture Analysis: Macrotexture, Microtexture, and Orientation Mapping, second ed., CRC Press, 2009.

[30] C. Rehrl, S. Kleber, T. Antretter, R. Pippan, A methodology to study crystal plasticity inside a compression test sample based on image correlation and EBSD, Mater. Char. 62 (2011) 793–800, https://doi.org/10.1016/j.matchar.2011.05.009.

[31] C. Caër, R. Pesci, Local behavior of an AISI 304 stainless steel submitted to in situ biaxial loading in SEM, Mater. Sci. Eng. 690 (2017) 44–51, https://doi.org/10.1016/j.msea.2017.02.087.

[32] T.R. Bieler, P. Eisenlohr, F. Roters, D. Kumar, D.E. Mason, M.A. Crimp, D. Raabe, The role of heterogeneous deformation on damage nucleation at grain boundaries in single phase metals, Int. J. Plast. 25 (2009) 1655–1683, https://doi.org/10.1016/j.ijplas.2008.09.002.